Supporting Information

Controllable CO_2 conversion via high performance proton conducting solid oxide electrolysis cell and the possible mechanisms

Nai Shi, [a]Yun Xie, [a] Daoming Huan, [a]Yi Yang, [a] Shuangshuang Xue, [a] Zeming Qi, [b] Yang Pan, [b] Ranran Peng,[acd] ChangrongXia, [a] Yalin Lu* [abcd]*

[a]CAS Key Laboratory of Materials for Energy Conversion, Department of Materials Science and Engineering, University of Science and Technology of China, Hefei, 230026 Anhui, China

[b]National Synchrotron Radiation Laboratory, University of Science and Technology of China, Hefei 230026, P. R. China

[c]Synergetic Innovation Center of Quantum Information & Quantum Physics, University of Science and Technology of China, Hefei, Anhui 230026, China

[d]Hefei National Laboratory of Physical Science at the Microscale, University of Science and Technology of China, Hefei, 230026 Anhui, China

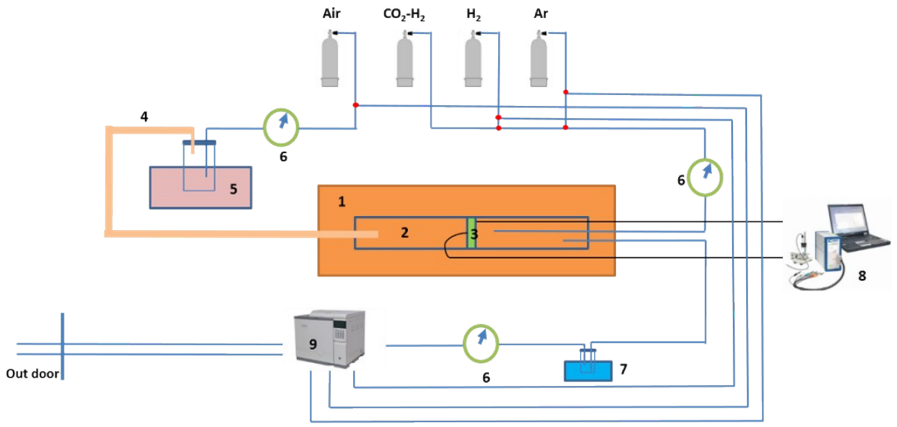

1.Furnace 2.Alumina tube 3.P-SOEC 4.Heater band 5.Water bath 6.Mass flowmeter 7.Cold trap 8.Electrochemical workstation 9. Gas chromatography

Figure S1. Schematic illustration of the testing system for proton conducting solid oxide electrolysis cells

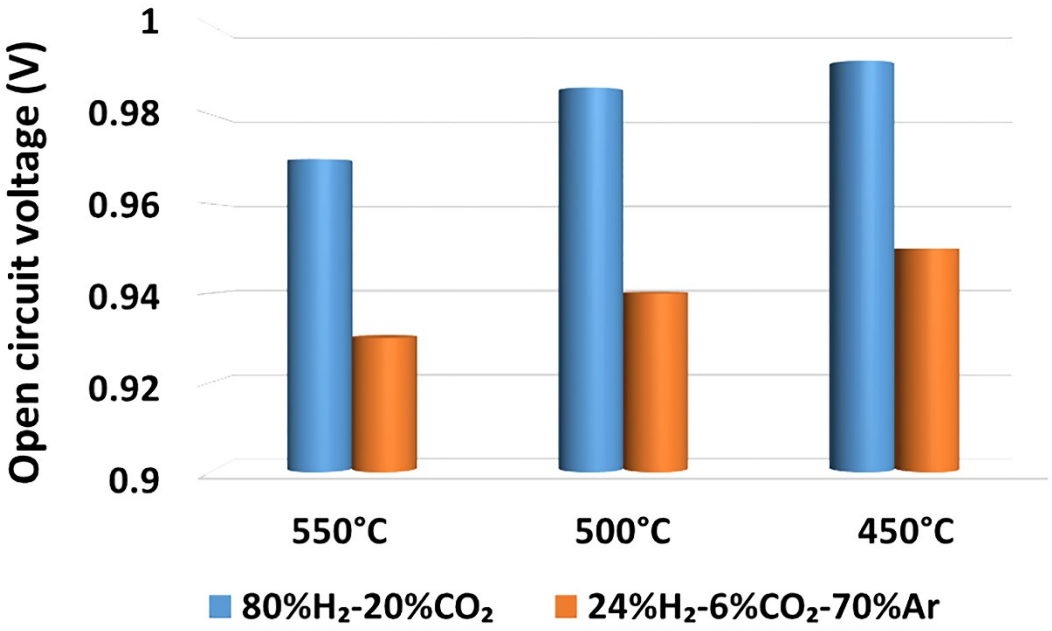

Figure S2. Open circuit voltages of single cell measured from 550 to 450 °C with 80 % H_2-20 % CO_2 (blue) and 24 % H_2-6 % CO_2-70 % Ar (orange) injected to the cathode, respectively.

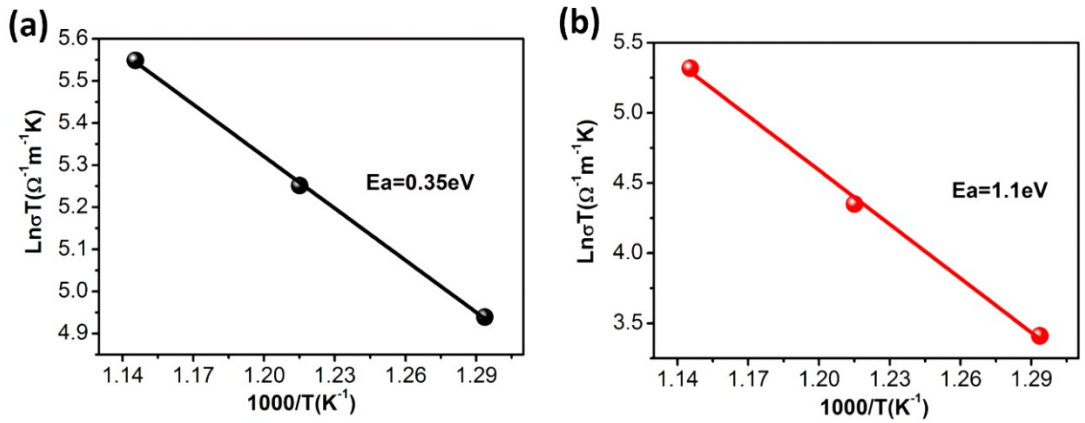

Figure S3. Temperature dependence of (a) R_b and (b) R_p of P-SOEC tested at OCV condition with 20 % CO_2- 80 % H_2 mixture in cathode. Activation energies for R_b and R_p are also calculated.

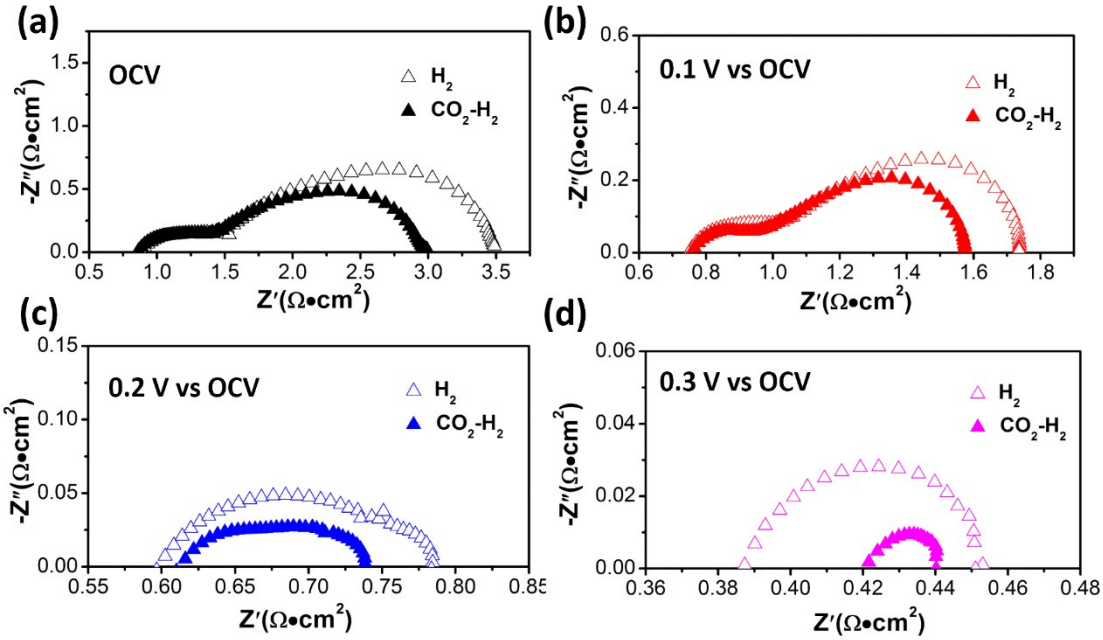

Figure S4. Impedance spectra of P-SOEC measured at 550 °C and electrolysis voltages of (a) 0 V, (b) 0.1 V, (c) 0.2 V, and (d) 0.3 V (vs. OCV) with H_2 (hollow) and H_2-CO_2 mixture (solid) injected to cathode.

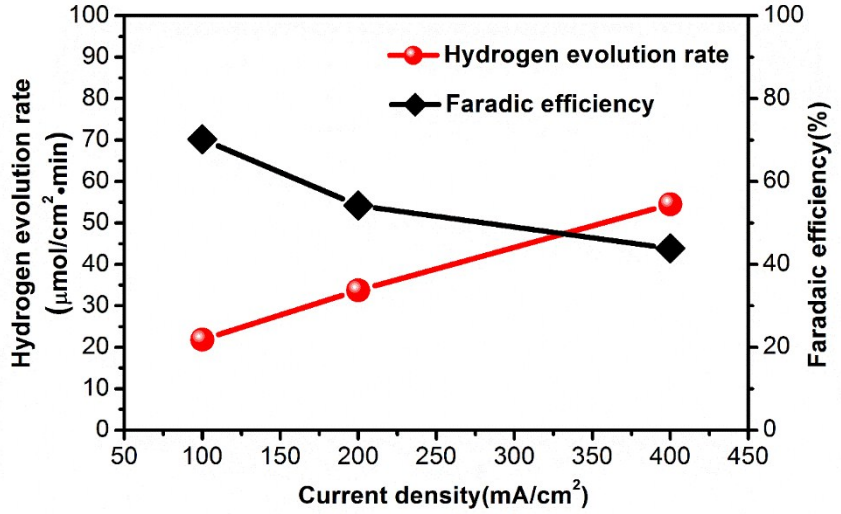

Figure S5. Hydrogen evolution rate (red) and Faradic efficiency (black) of pure steam electrolysis in P-SOEC as function of electrolysis current density measured at 550 ^{o}C.

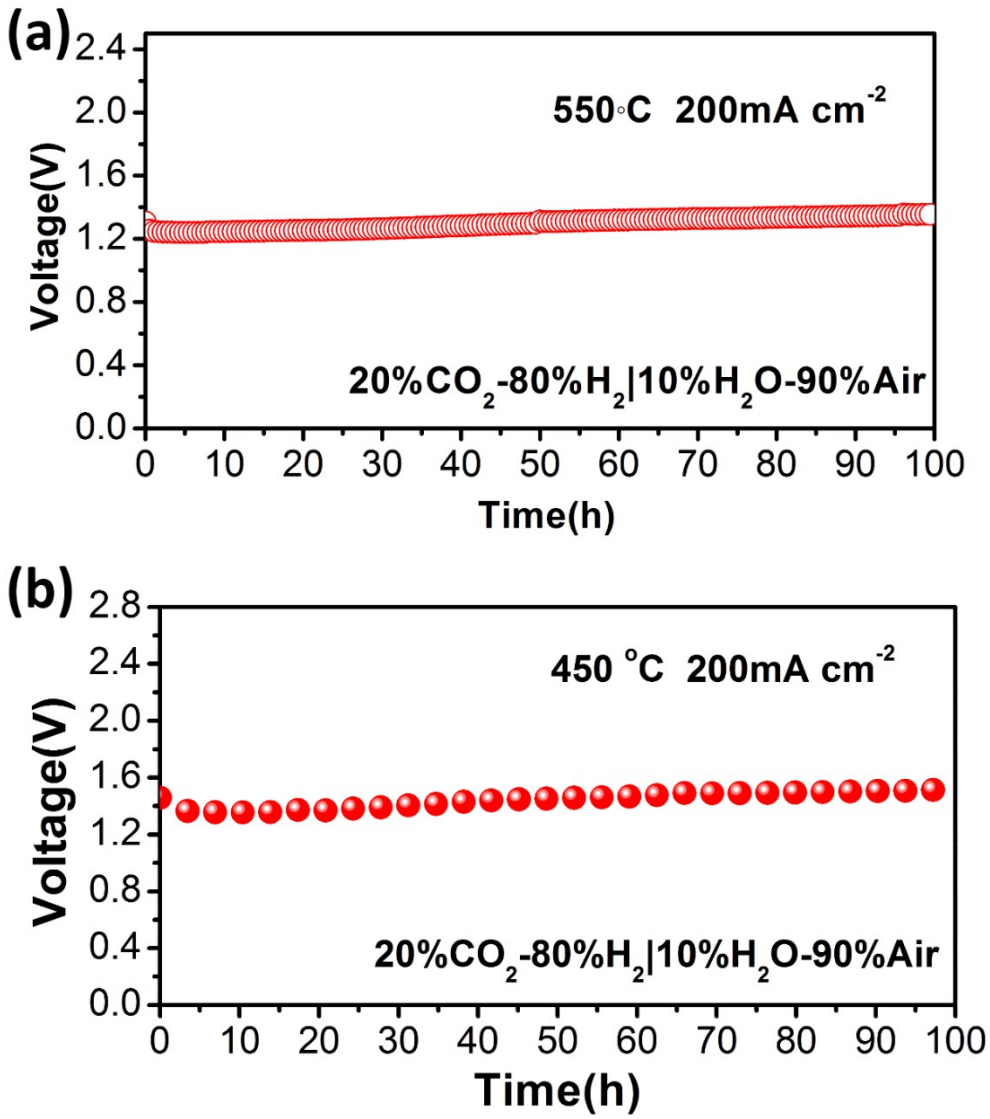

Figure S6. Long term stability of CO_2 conversion via P-SOEC measured at (a) 550 ^oC and (b) 450 ^oC under an electrolysis current density of 200 mA cm^{-2}.

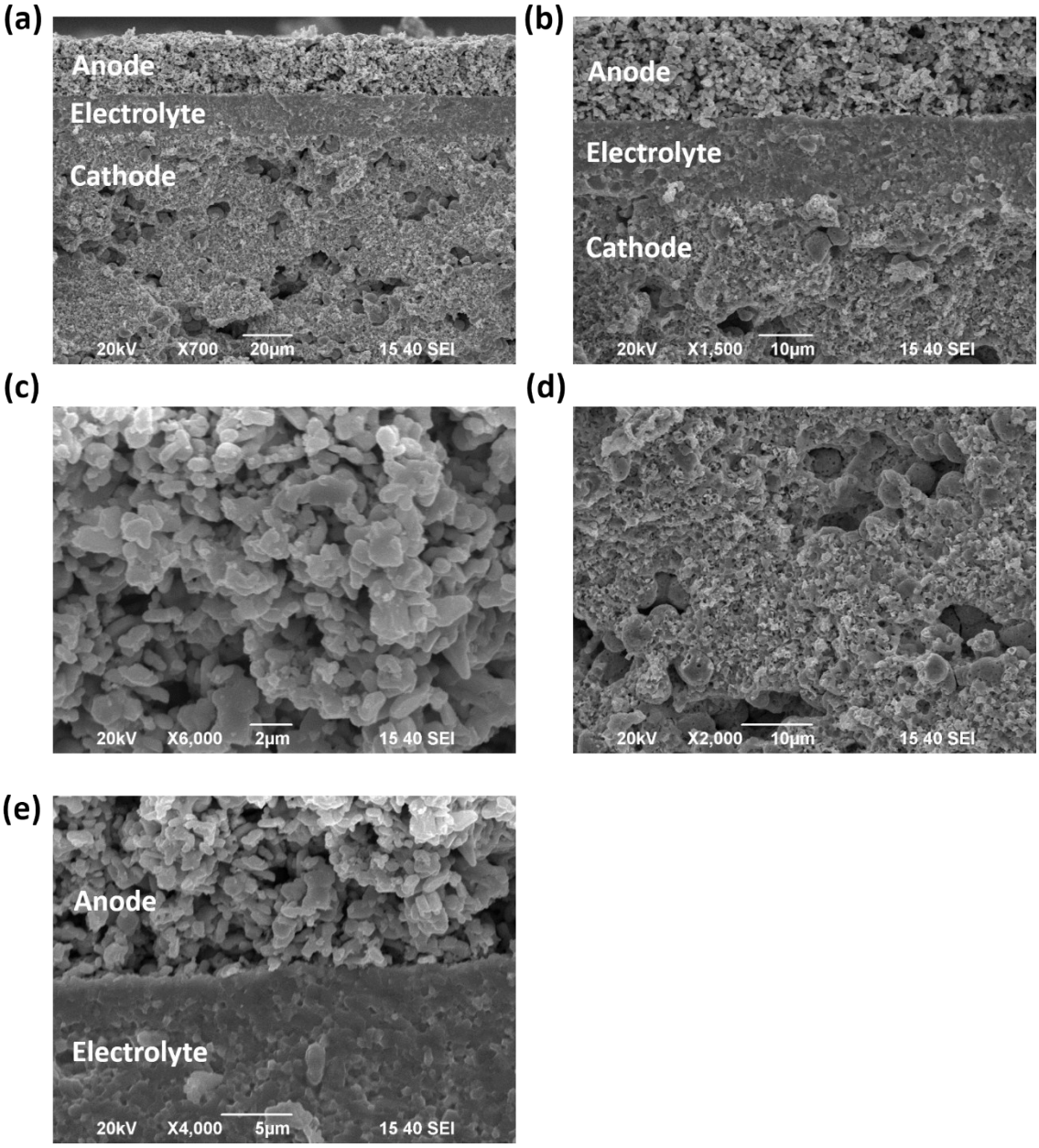

Figure S7. SEM pictures of fractured single cell after testing at 450 ^{o}C for 100 hours: (a) overview of single cell, (b) enlarged view of the interface between electrode and electrolyte, (c) enlarged view of anode, (d) enlarged view of cathode and (e) enlarged view of electrolyte and anode.

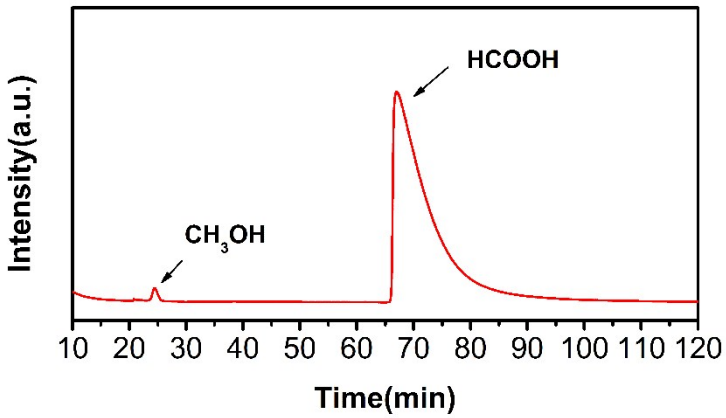

Figure S8. Composition of condensed liquid for cathode outlet gas.

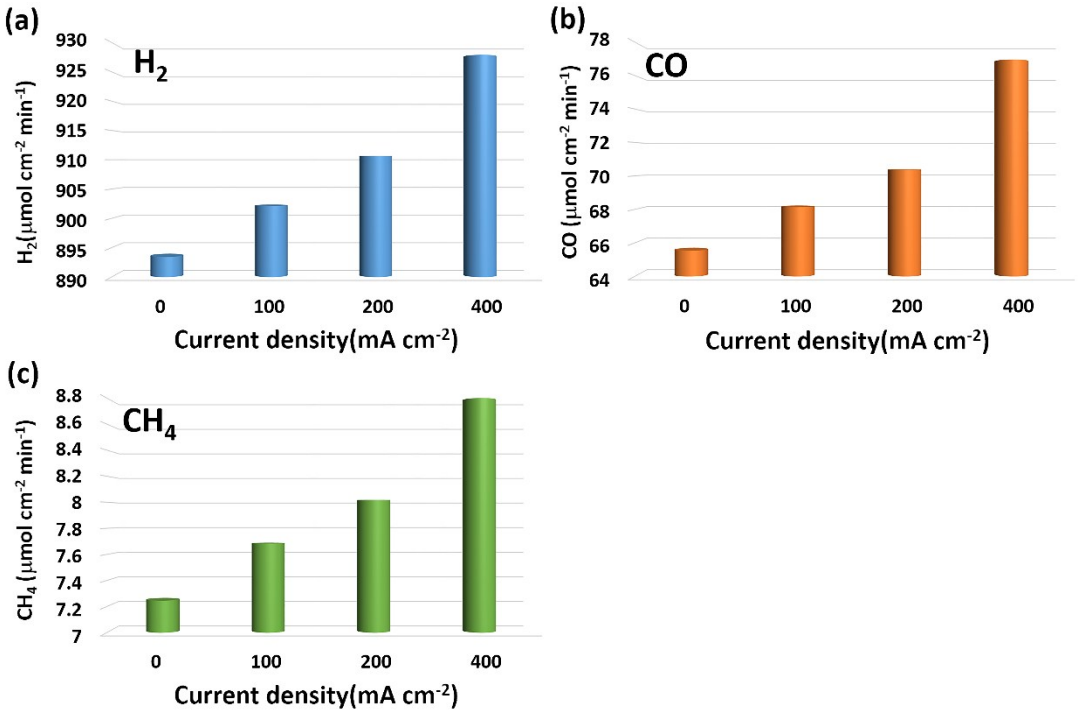

Figure S9. Flow rates of (a) H_2, (b) CO and (c) CH_4 in cathode outlet gas as function of applied current densities measured at 550 ^oC.

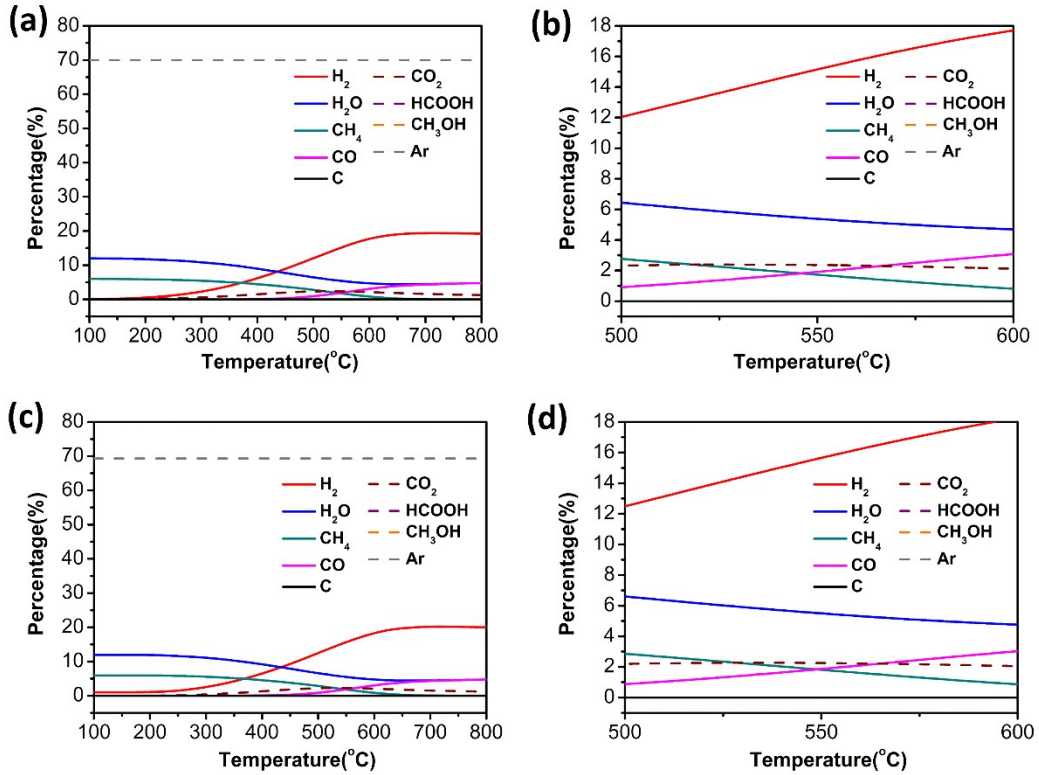

Figure S10. Temperature dependence of (a) theoretical equilibrium composition and (b) its enlarged view for the original gas of 6 % CO_2-24 % H_2-70 % Ar. Temperature dependence of (c) theoretical equilibrium composition and (d) its enlarged view for the gas with additional 0.469 % H_2 in 6 % CO_2-24 % H_2-70 % Ar mixture.

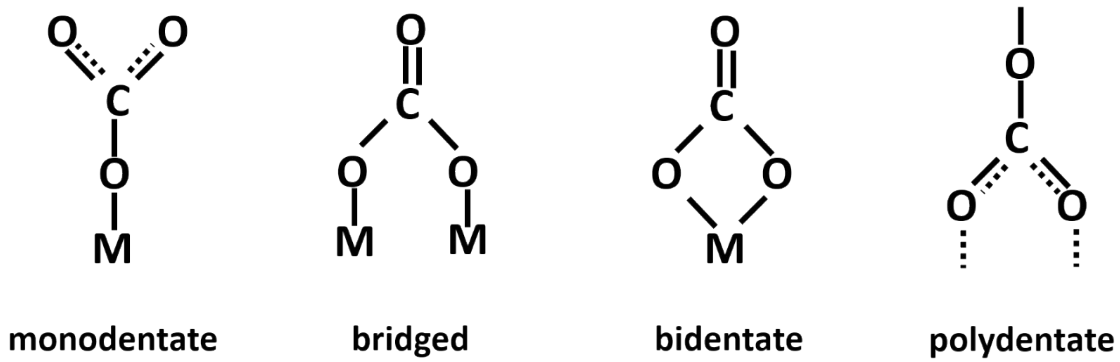

Figure S11. Illustration of various carbonate configurations

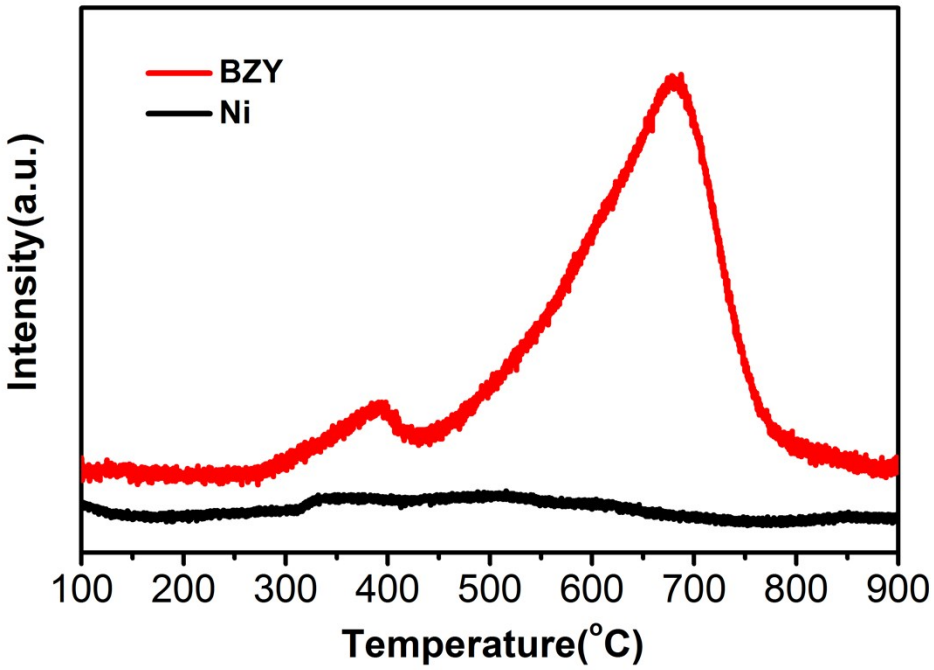

Figure S12. CO_2-TPD spectrum of BZY and nickel powders.

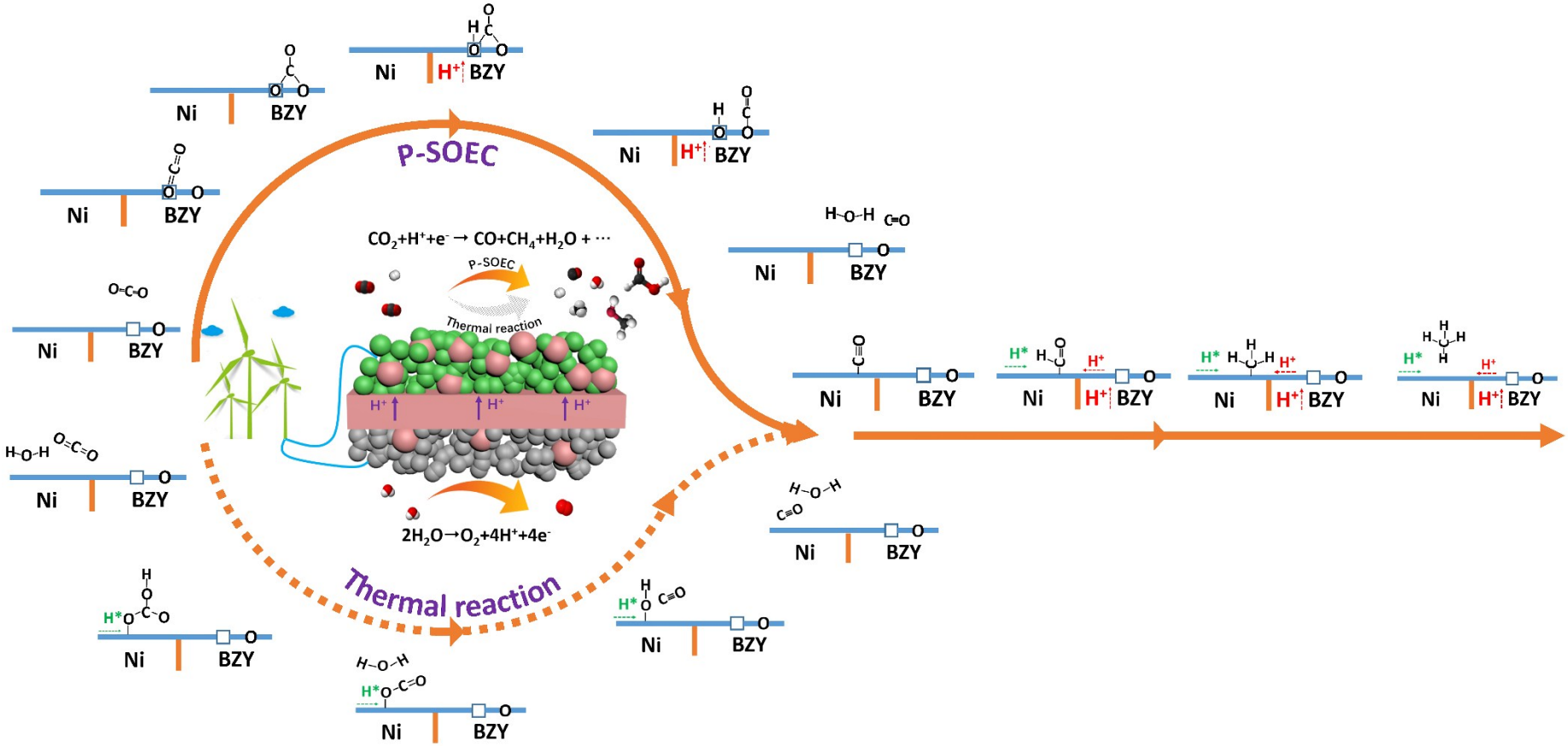

Figure S13. Possible schematic diagram of CO_2 reduction reactions in P-SOEC. H^+(red) indicates the protons transferred from anode, H*(green) indicates the hydrogen atoms from hydrogen dissociation in nickel.

Table S1. Performance of SOECs reported in the literature in similar test conditions. BCZYZ ($BaCe_{0.5}Zr_{0.3}Y_{0.16}Zn_{0.04}O_3$), LSMC ($(La_{0.75}Sr_{0.25})_{0.95}Mn_{0.5}Cr_{0.5}O_3$), CMF ($Ce_{0.6}Mn_{0.3}Fe_{0.1}O_2$) LSFM ($La_{0.6}Sr_{0.4}Fe_{0.9}Mn_{0.1}O_3$), LSCF ($La_{0.6}Sr_{0.4}Co_{0.2}Fe_{0.8}O_3$), GDC ($Gd_{0.2}Ce_{0.8}O_2$), BZCYYZ ($BaZr_{0.1}Ce_{0.7}Y_{0.1}Yb_{0.06}Zn_{0.04}O_3$), BCZDy ($BaCe_{0.3}Zr_{0.5}Dy_{0.2}O_3$), NBN ($Nd_{1.95}Ba_{0.05}NiO_4$), BZY ($BaZr_{0.8}Y_{0.2}O_3$), SFM ($Sr_2Fe_{1.5}Mo_{0.5}O_6$), BZCY5 ($BaZr_{0.3}Ce_{0.5}Y_{0.2}O_3$), SEFC ($SrEu_2Fe_{1.8}Co_{0.2}O_7$) YSZ ($Zr_{0.85}Y_{0.15}O_2$), LSM ($La_{0.8}Sr_{0.2}MnO_3$), BZCY7 ($BaCe_{0.7}Zr_{0.1}Y_{0.2}O_3$), LSN ($La_{1.2}Sr_{0.8}NiO_4$), PNO ($Pr_2NiO_4$), BZCY6 ($BaZr_{0.2}Ce_{0.6}Y_{0.2}O_3$), NBSCF ($NdBa_{0.5}Sr_{0.5}Co_{1.5}Fe_{0.5}O_6$)

Single cell configuration (cathode|electrolyte|anode)	**Test atmosphere (cathode|anode)**	**Open circuit voltage(V)**	**Applied Voltage (V)**	**Stability test**	**Current density (A/cm^2)**	**Year/ reference**
Ni-BCZYZ|BCZYZ|LSMC-BCZYZ	CO_2|5%H_2O-95%Ar	0.1 (600 °C)	2	12h	0.1	2013[1]
CMF-LSFM/LSCF+GDC|BZCYYZ|Ni-Fe	CO_2|3%H_2O-97%H_2	0 (600 °C)	1.3	_	0.25	2015[2]
Fe-BCZYZ|BCZYZ| Ni-BCZYZ	CO_2|3%H_2O-97%H_2	0 (614 °C)	2.6	1h	1.5	2011[3]
Ni-BCZDy|BCZDy|NBN-BCZDy	50%CO_2-50%H_2 |30%H_2O-70%Air	0.8 (700 °C)	1.5	10h	1	2018[4]
Ni-BZY|BZY|BZY-SFM	90%N_2-10%H_2 |3%H_2O-97%Air	0.92 (550 °C)	1.3	100h	0.1	2017[5]
Ni-BZY|BZY|BZY-LSCF	96%Ar-4%H_2 |3%H_2O-97%Air	0.86 (600 °C)	1.32	80h	0.055	2015[6]
Ni-BZCY5|BZCY5|BZCY5-SEFC	3%H_2O-97%H_2 |10%H_2O-90%Air	0.99 (600 °C)	1.5	230h	1.05	2018[7]
Ni-YSZ|YSZ|YSZ-LSM	11.4%CO_2-68.6%H_2-	0.09 (800 °C)	1.3	24h	0.4	2014[8]

	20%H_2O|Air					
$BaCO_3$ modified Ni-YSZ|YSZ|YSZ-LSM	20%CO_2-80%H_2|Air	0.05 (800 °C)	1.3	280h	0.69	2018[9]
Ni-BZCY7|BZCY7|LSN	3%H_2O-97%H_2|20%H_2O-80%Air	0.98 (700 °C)	1.3	40h	1.37	2018[10]
Ni-BZCY6|BZCY6|PNO-BZCY6	H_2|40%H_2O-60%Air	1 (600 °C)	1.5	_	0.6	2018[11]
Ni-BZCYYb|BZCYYb|NBSCF-BZCYYb	10%H_2O-90%H_2|10%H_2O-90%Air	1.03 (550 °C)	1.3	60h	0.42	2018[12]
Ni-BZY|BZY|BZY-SEFC	20%CO_2-80%H_2 |10%H_2O-90%Air	0.94 (600 °C)	1.5	100h	1.73	This work
			1.3		0.76	
		0.97 (550 °C)	1.5		1.23	
			1.3		0.45	
		1 (450 °C)	1.5		0.41	
	6%CO_2-24%H_2-70%Ar|10%H_2O-90%Air	0.93 (550 °C)	1.3		0.2	

Calculations

1. Selectivity

The selectivity of CO and CH_4 are calculated by the equation (1):

$$Selectivity(\%) = \frac{mole\ of\ target\ product * carbon\ atoms\ in\ molecular\ formula}{mole\ of\ reacted\ CO_2} * 100\% \quad (1)$$

2. Faradic efficiency

The faradic efficiency is calculated by equation (2):

$$\eta = \frac{mnF}{It} \tag{2}$$

where n is mole of hydrogen, I is current, t is time, m is transport number of electron, and F is faradic constant

2. Thermal equilibrium composition calculation

Thermal equilibrium gas composition is calculated through minimize Gibbs method (equation.3):

$$G(n_i) = \sum_i^k n_i \mu_i \tag{3}$$

Where n_i is the mole of species *i* and μ_i is the chemical potential of species *i.* Take the derivation of n_i, and at the equilibrium state, there should be:

$$d(G_{system})_{T,P} = 0 \tag{4}$$

Achieving n_i by solving equation (4).

Assuming the Faradaic efficiency is 43.8% at the electrolysis current density of 400mAcm^2, and the calculated hydrogen production is 1.22 ml/min·cm^2 according to equation (5):

$$n = \frac{\eta I t}{mF} \tag{5}$$

where n is mole of hydrogen, I is current, t is time, m is transport number of electron, and F is faradic constant. Considering the effective area in our single cell is 0.38465 cm^2, 0.469 ml/min hydrogen should be added to simulate the electrolysis system.

Reference

[1] G. Wu, K. Xie, Y. Wu, W. Yao and J. Zhou, *J. Power Sources*, 2013, **232**, 187-192.

[2] T.H. Shin, J.-h. Myung, K.M. Naeem, C. Savaniu and J.T. Irvine, *Solid State Ionics*, 2015, **275**, 106-109.

[3] K. Xie, Y. Zhang, G. Meng and J.T. Irvine, *J. Mater. Chem.*, 2011, **21**, 195-198.

[4] N. Danilov, A. Tarutin, J. Lyagaeva, G. Vdovin and D. Medvedev, *J. Mater. Chem. A*, 2018, **6**, 16341-16346.

[5] L. Lei, Z. Tao, X. Wang, J.P. Lemmon and F. Chen, *J. Mater. Chem. A*, 2017, **5**, 22945-22951.

[6] L. Bi, S.P. Shafi and E. Traversa, *J. Mater. Chem. A*, 2015, **3**, 5815-5819.

[7] D. Huan, N. Shi, L. Zhang, W. Tan, Y. Xie, W. Wang, C. Xia, R. Peng and Y. Lu, *ACS Appl. Mater. Interfaces*, 2018, **10**, 1761-1770.

[8] L. Chen, F. Chen and C. Xia, *Energy Environ. Sci.*, 2014, **7**, 4018-4022.

[9] M. Zheng, S. Wang, Y. Yang and C. Xia, *J. Mater. Chem. A*, 2018, **6**, 2721-2729.

[10] S. Yang, Y. Wen, J. Zhang, Y. Lu, X. Ye and Z. Wen, *Electrochim. Acta*, 2018, **267**, 269-277.

[11] W. Li, B. Guan, L. Ma, S. Hu, N. Zhang and X. Liu, *J. Mater. Chem. A*, 2018, **6**, 18057-18066.

[12] J. Kim, A. Jun, O. Gwon, S. Yoo, M. Liu, J. Shin, T. H. Lim and G. Kim, *Nano Energy*, 2018, **44**, 121-126.

.